Geophysical Research Letters

RESEARCH LETTER
10.1029/2018GL079095

Key Points:
- Three ion-scale flux ropes with varying axial directions were observed near a magnetotail x-line encounter
- An intense, localized electric field within one of the flux ropes is associated with an electron-scale vortex
- The electron vortex is associated with a magnetic field that is frozen-in to the electron flow and a small-scale magnetic enhancement

Correspondence to:
J. E. Stawarz,
j.stawarz@imperial.ac.uk

Citation:
Stawarz, J. E., Eastwood, J. P., Genestreti, K. J., Nakamura, R., Ergun, R. E., Burgess, D., et al. (2018). Intense electric fields and electron-scale substructure within magnetotail flux ropes as revealed by the Magnetospheric Multiscale mission. *Geophysical Research Letters*, *45*, 8783–8792. https://doi.org/10.1029/2018GL079095

Received 5 JUN 2018
Accepted 17 AUG 2018
Accepted article online 24 AUG 2018
Published online 12 SEP 2018

Intense Electric Fields and Electron-Scale Substructure Within Magnetotail Flux Ropes as Revealed by the Magnetospheric Multiscale Mission

J. E. Stawarz[1], J. P. Eastwood[1], K. J. Genestreti[2], R. Nakamura[2], R. E. Ergun[3,4], D. Burgess[5], J. L. Burch[6], S. A. Fuselier[6,7], D. J. Gershman[8], B. L. Giles[8], O. Le Contel[9], P.-A. Lindqvist[10], C. T. Russell[11], and R. B. Torbert[12]

[1]Department of Physics, Imperial College London, London, UK, [2]Space Research Institute, Austrian Academy of Sciences, Graz, Austria, [3]Department of Astrophysical and Planetary Sciences, University of Colorado Boulder, Boulder, CO, USA, [4]Laboratory for Atmospheric and Space Physics, University of Colorado Boulder, Boulder, CO, USA, [5]School of Physics and Astronomy, Queen Mary University of London, London, UK, [6]Southwest Research Institute, San Antonio, TX, USA, [7]University of Texas at San Antonio, San Antonio, TX, USA, [8]NASA Goddard Space Flight Center, Greenbelt, MD, USA, [9]Laboratoire de Physique des Plasmas, CNRS, Ecole Polytechnique, Sorbonne Université, Université Paris Sud, Observatoire de Paris, Paris, France, [10]School of Electrical Engineering, KTH Royal Institute of Technology, Stockholm, Sweden, [11]Department of Earth, Planetary, and Space Sciences, University of California, Los Angeles, CA, USA, [12]Department of Physics, University of New Hampshire, Durham, NH, USA

Abstract Three flux ropes associated with near-Earth magnetotail reconnection are analyzed using Magnetospheric Multiscale observations. The flux ropes are Earthward propagating with sizes from ~3 to 11 ion inertial lengths. Significantly different axial orientations are observed, suggesting spatiotemporal variability in the reconnection and/or flux rope dynamics. An electron-scale vortex, associated with one of the most intense electric fields (**E**) in the event, is observed within one of the flux ropes. This **E** is predominantly perpendicular to the magnetic field (**B**); the electron vortex is frozen-in with **E** × **B** drifting electrons carrying perpendicular current and causing a small-scale magnetic enhancement. The vortex is ~16 electron gyroradii in size perpendicular to **B** and potentially elongated parallel to **B**. The need to decouple the frozen-in vortical motion from the surrounding plasma implies a parallel **E** at the structure's ends. The formation of frozen-in electron vortices within reconnection-generated flux ropes may have implications for particle acceleration.

Plain Language Summary The release of magnetic energy into particle motion through magnetic reconnection is a key driver of dynamics in the Earth's magnetosphere and other space plasmas. In order to understand how the released magnetic energy is distributed and ultimately heats the particles, a detailed examination of the structures formed by magnetic reconnection is necessary. One common structure produced by reconnection is a twisted magnetic field known as a flux rope. We use new data from the National Aeronautics and Space Administration's Magnetospheric Multiscale satellites to examine both the large- and small-scale properties of three flux ropes associated with a single reconnection event. The results reveal the intrinsic three-dimensional nature of the overall reconnection event, which may stem either from variability at the reconnection site and/or the subsequent dynamics of the structures after they form. Additionally, the high-resolution measurements reveal a new small-scale structure, namely, a vortex of electrons, inside of one of the flux ropes. The presence of such vortices may contribute to accelerating particles and points to the necessity of better understanding the substructure of flux ropes in order to characterize particle energization in magnetic reconnection.

1. Introduction

Magnetic reconnection is a key driver of dynamics in Earth's magnetosphere, both at the dayside magnetopause and the magnetotail. In the magnetotail, near-Earth reconnection occurs ~25R_E from Earth. The resulting reconnection jets transport energy and drive dynamics in the plasma sheet (Sergeev et al., 2012; Stawarz et al., 2015) and plasma waves excited by reconnection transport energy to the auroral region (Shay et al., 2011; Stawarz et al., 2017). Understanding the structures and small-scale physics driven by

reconnection is necessary to answer fundamental questions about reconnection and energy transport in Earth's magnetosphere.

Magnetic flux ropes are one type of structure associated with reconnection and are observed in many space plasmas, including Earth's plasma sheet (Borg et al., 2012; Eastwood & Kiehas, 2015; Sharma et al., 2008). These helical magnetic field (**B**) structures can be generated between two distinct x-lines, either between near-Earth and distant tail x-lines (Hones, 1977; Hughes & Sibeck, 1987) or two near-Earth x-lines (Eastwood et al., 2005). Alternatively, they can form as secondary islands, generated by the instability of a single x-line (Daughton et al., 2006; Drake, Swisdak, Schoeffler, et al., 2006) or an electron Kelvin-Helmholtz instability near the separatrix (Fermo et al., 2012), which are transported away from the x-line within the reconnection outflows (Eastwood et al., 2007; Fear et al., 2008; Wang et al., 2010). Flux ropes may facilitate particle acceleration (Dahlin et al., 2017; Drake, Swisdak, Che, et al., 2006) and are observationally linked with enhanced energetic electrons (Chen et al., 2008), making accurate descriptions of flux ropes imperative for understanding energy partition and particle acceleration in reconnection.

The simplest model of a flux rope is a force-free field, where current is aligned with **B** such that the Lorentz force is 0 (Lundquist, 1950). The force-free model reasonably describes some flux ropes observed in the plasma sheet (Slavin, Lepping, Gjerloev, Fairfield, et al., 2003; Yang et al., 2014) and, at Earth's magnetopause, reasonably describes even ion-scale flux ropes (Eastwood et al., 2016). However, additional substructure has been noted. Slavin, Lepping, Gjerloev, Goldstein, et al. (2003) demonstrated large deviations in the alignment of the current with **B** in a plasma sheet flux rope, indicating nonforce-free behavior. Enhanced wave activity, including electrostatic, whistler, and kinetic Alfvén waves, has been observed within flux ropes (Kennel et al., 1986; Øieroset et al., 2014; Wang et al., 2016). Additionally, large electric fields (**E**), approaching 100 mV/m, have been observed (Eastwood et al., 2007). While the nature of these **E** have not been observationally characterized, simulations show **E** within flux ropes with profiles depending on the formation mechanism (Chen et al., 2012; Huang et al., 2014; Zhou et al., 2012).

The Magnetospheric Multiscale (MMS) mission (Burch et al., 2016), with high-time-resolution, multispacecraft measurements at separations approaching electron scales, can directly probe electron-scale substructure within flux ropes. In this study, MMS data are used to examine three flux ropes associated with a magnetotail reconnection event. An electron vortex is discovered, associated with one of the most intense **E** in the entire reconnection event. Such a vortex has not been previously reported within a flux rope, although similar structures have been identified in other plasma environments. Section 2 gives an overview of the data and event. Section 3 characterizes the large-scale structure of the flux ropes. Section 4 discusses the small-scale substructure with focus on the electron vortex. Results are compared and contrasted with observations and theory of similar electron vortices, and implications for the dynamics within flux ropes are discussed.

2. Observations

On 11 July 2017 at ~22:34 universal time coordinated (UTC), while MMS was ~22R_E down tail from Earth, the electron diffusion region (EDR) of a near-Earth magnetotail reconnection event was encountered (Torbert et al., 2017). Shortly after the EDR, MMS observed three flux ropes. We examine these flux ropes using **B** measurements from the fluxgate (Russell et al., 2016) and searchcoil (Le Contel et al., 2016) magnetometers, **E** measurements from the electric field double probes (Ergun et al., 2016; Lindqvist et al., 2016), and plasma moments, such as the ion ($\mathbf{V}_i$) and electron ($\mathbf{V}_e$) velocities, from the Fast Plasma Investigation (FPI; Pollock et al., 2016) and Hot Plasma Composition Analyzer (Young et al., 2016). The spacecraft are separated by ~15 km, which is approximately the electron inertial length (d_e) and much smaller than the ion inertial length (d_i) of ~540 km. The thermal electron gyroradius (ρ_e) is ~10 km.

The tetrahedral formation of MMS allows computation of the current density (**J**) using the curlometer technique (Robert et al., 1998). **J** can also be computed from plasma measurements using $\mathbf{J} = n_e q(\mathbf{V}_i - \mathbf{V}_e)$, where n_e is the electron number density, and q is the proton charge. Quasineutrality is assumed such that the higher resolution n_e is appropriate for computing **J**. Computing **J** from plasma moments gives independent measurements for each spacecraft, which can be compared with the curlometer by interpolating to the formation's barycenter.

Figure 1 gives an overview of the flux ropes and reconnection event in geocentric solar magnetospheric (GSM) coordinates. At ~22:34:03 UTC, a local minimum in |**B**| is observed with tailward to Earthward V_{ex} and V_{ix}

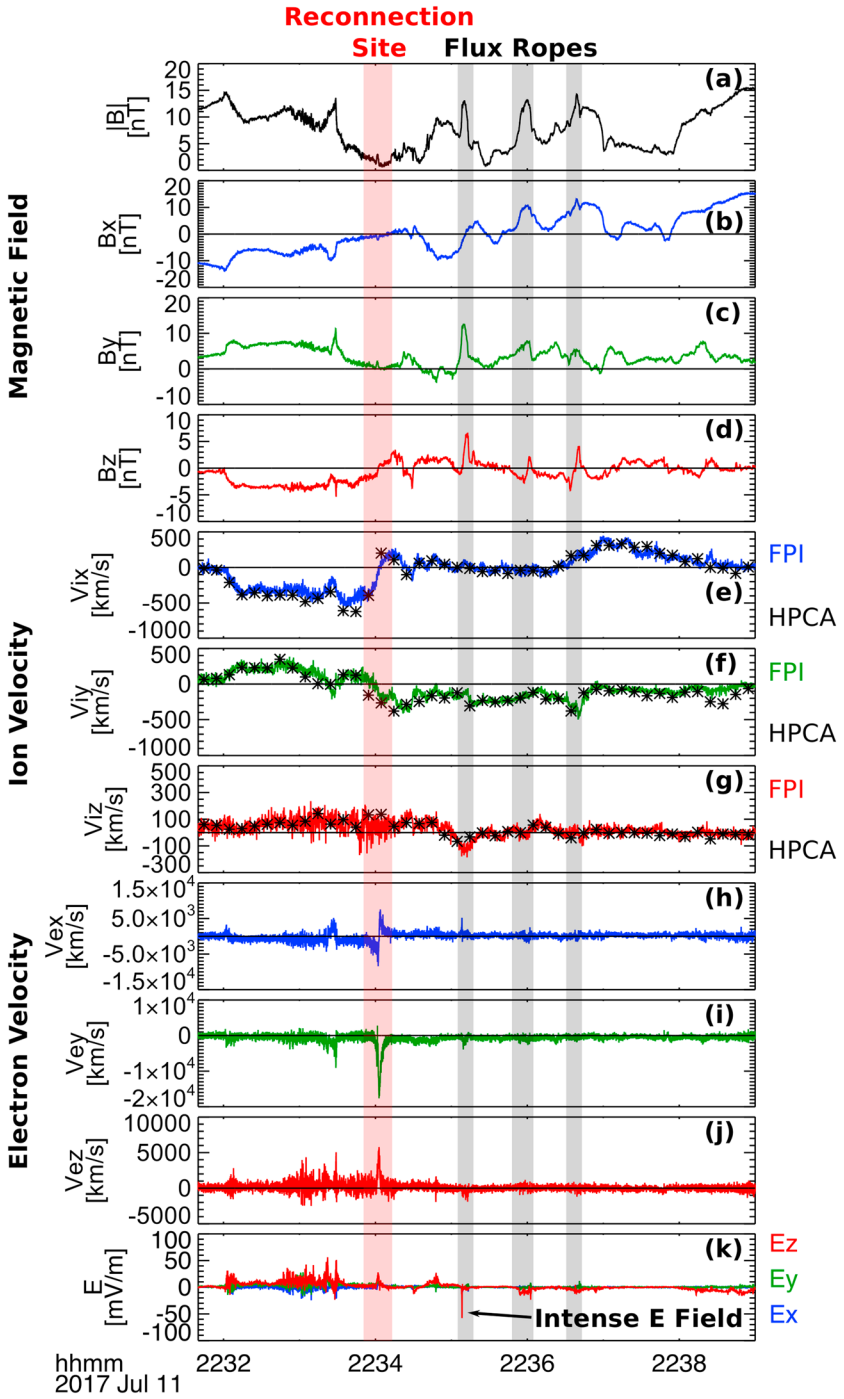

Figure 1. Overview of the reconnection event as observed by Magnetospheric Multiscale 1 showing (a–d) the magnitude and components of **B**, (e–g) $\mathbf{V}_i$ as measured by FPI and HPCA, (h–j) $\mathbf{V}_e$, and (k) **E**. All vectors are in geocentric solar magnetospheric coordinates. Three flux ropes (gray shaded) are observed after an x-line encounter (pink shaded). One of the strongest **E** in the event is observed within the first flux rope. FPI = Fast Plasma Investigation; HPCA = Hot Plasma Composition Analyzer.

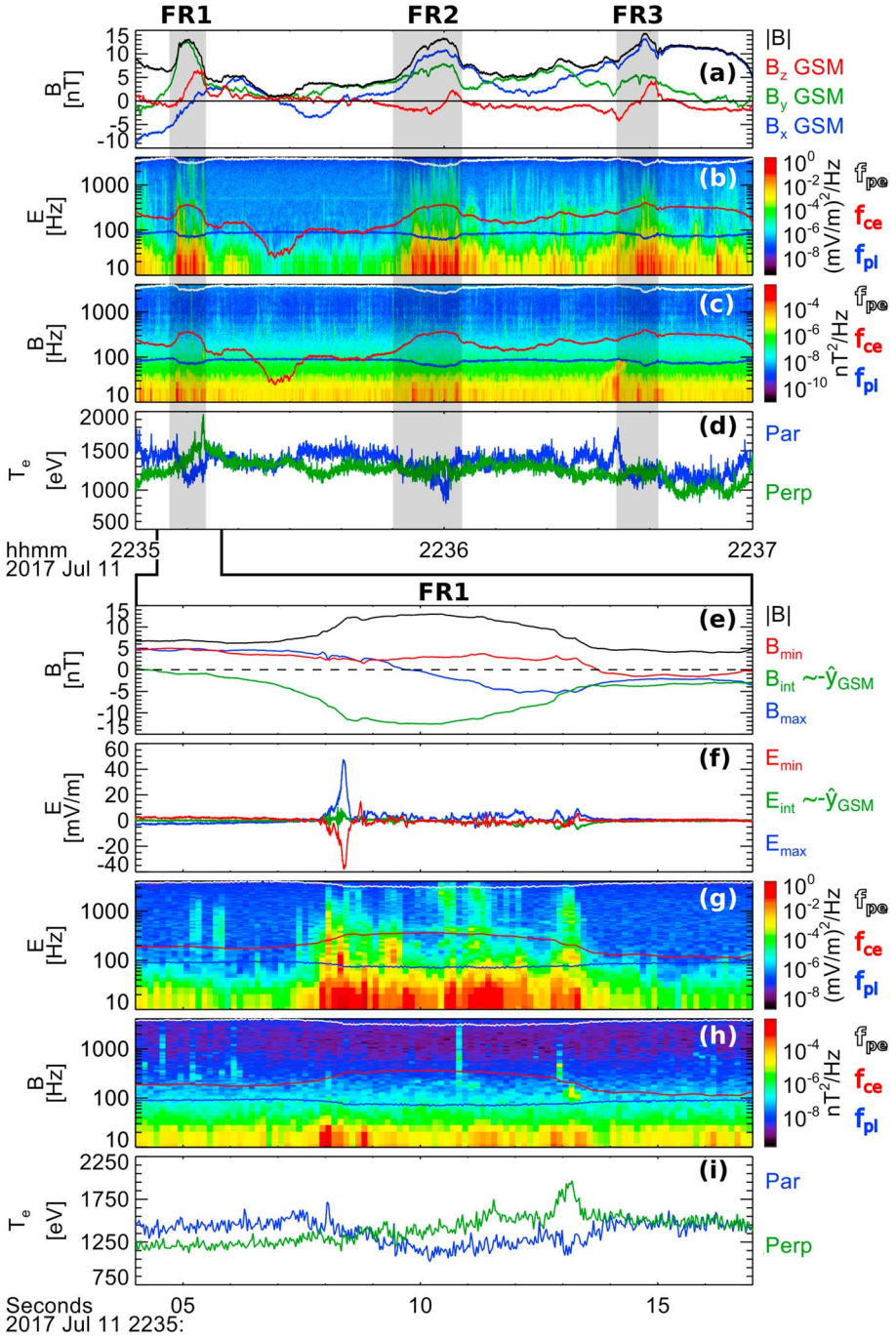

Figure 2. Overview of the three flux ropes (gray shaded) showing (a) the magnitude and components of **B** in GSM coordinates, (b) spectrogram of **E**, (c) spectrogram of **B**, and (d) parallel and perpendicular electron temperature. Enlarged view of FR1 showing (e) the magnitude and components of **B** in minimum variance coordinates based on **B** between 22:35:07 and 22:35:13.5 universal time coordinated, (f) **E** in the same minimum variance coordinate system, and (g–i) same as (b–d). The electron plasma frequency, electron cyclotron frequency, and ion plasma frequency are plotted as white, red, and blue curves, respectively, on the spectrograms. GSM = geocentric solar magnetospheric; FR = flux rope.

Table 1
Flux Rope Orientations and Sizes

	Axial direction [GSM]		Tilt[a]		Velocity[b]	Size	
	MVA	Timing	MVA	Timing	(km/s)	(km)	(d_i)
FR1	[0.06, 0.996, 0.07]	[0.51, 0.82, 0.25]	3°	32°	256 [0.61, −0.32, −0.73]	1,740	3.2
FR2	[0.93, 0.34, 0.13]	[0.98, 0.19, 0.001]	70°	79°	451 [0.29, −0.94, −0.19]	6,010	11
FR3	[0.83, 0.55, 0.09]	[0.95, 0.26, −0.18]	56°	75°	501 [0.24, −0.92, 0.32]	3,910	7.1

Note. GSM = geocentric solar magnetospheric; MVA = minimum variance analysis; FR = flux rope.
[a]Angle between $\hat{\mathbf{y}}_{GSM}$ and axial direction in $\hat{\mathbf{x}}_{GSM}$-$\hat{\mathbf{y}}_{GSM}$ plane. [b]Velocity perpendicular to axial direction in GSM coordinates.

reversals and a southward to northward B_z reversal, consistent with crossing from tailward to Earthward of a magnetotail reconnection event. The intense negative, unipolar V_{ey} at the same time is the signature of the thin reconnecting cross-tail current sheet. The traversal of the reconnection site involved an EDR encounter (Torbert et al., 2017). A large-scale, tailward to Earthward V_{ix} reversal is observed between 22:32 and 22:38 UTC. FPI and Hot Plasma Composition Analyzer measurements of $\mathbf{V}_i$ reasonably agree, although $\mathbf{V}_i$ may be underestimated by a factor of two due to ion distributions extending above the FPI energy range (Torbert et al., 2017).

In the middle of the large-scale $\mathbf{V}_i$ reversal, three flux ropes, characterized by localized |**B**| enhancements and bipolar B_z, are observed at 22:35:10, 22:36:00, and 22:36:38 UTC, referred to as FR1, FR2, and FR3, respectively. Figure 2a shows magnetic profiles of the flux ropes on a shorter timescale. The southward to northward B_z polarity is consistent with Earthward propagation. Based on the tailward x-line velocity of 170 km/s inferred from timing analysis (Torbert et al., 2017), these flux ropes are roughly 20, 40, and 50 d_i from the x-line. FR1 contains a localized **E** spike of ∼60 mV/m, which is among the largest **E** in the entire event and is explored further in section 4.1.

3. Large-Scale Flux Rope Properties

The orientation of the flux rope axes can be estimated with a single spacecraft using minimum variance analysis (MVA), where **B** is rotated into a coordinate system such that $\hat{x}_{min}$, $\hat{x}_{int}$, and $\hat{x}_{max}$ are directions of minimum, intermediate, and maximum variation, respectively (Sonnerup & Scheible, 1998). It is assumed one component will have a large unipolar variation and is the axial direction. However, the magnetic profile obtained will depend on the spacecraft trajectory and flux rope structure, with a straight line through the center giving the most accurate results (Eastwood et al., 2012; Kiehas et al., 2012; Lepping et al., 1990). Figure 2e shows FR1 in MVA coordinates, where $\hat{x}_{int} \sim -\hat{y}_{GSM}$ is the axial direction.

Another method for determining the orientation uses multispacecraft timing analysis on |**B**| (Schwartz, 1998). Assuming an axially invariant flux rope, the changes in |**B**| will be the boundaries in the flux rope cross section, and timing can be used to determine normal directions for the leading ($\hat{\mathbf{n}}_{in}$) and trailing ($\hat{\mathbf{n}}_{out}$) boundaries of the cross section. Here timing is based on when each spacecraft reaches a specified |**B**| amplitude, and the amplitude is varied to ensure consistent results for each boundary. Assuming $\hat{\mathbf{n}}_{in}$ is not parallel to $\hat{\mathbf{n}}_{out}$, the axial direction is given by $\hat{\mathbf{n}}_{in} \times \hat{\mathbf{n}}_{out}/|\hat{\mathbf{n}}_{in} \times \hat{\mathbf{n}}_{out}|$.

Table 1 summarizes the axial directions for each flux rope. Both methods show the flux ropes have different orientations, predominantly in the $\hat{x}_{GSM} - \hat{y}_{GSM}$ plane, with FR2 and FR3 tilted more toward $\hat{x}_{GSM}$ than FR1. This conclusion is consistent with magnetic profiles in Figure 2a, where FR1 shows a clear axial field signature in $B_{y,GSM}$, while FR2 and FR3 have indications of the axial field in $B_{x,GSM}$. The tilt is quantified in columns 4 and 5 of Table 1 in terms of the angle between $\hat{y}_{GSM}$ and the axial direction in the $\hat{x}_{GSM} - \hat{y}_{GSM}$ plane. Relative angles between $\hat{\mathbf{n}}_{in}$ and $\hat{\mathbf{n}}_{out}$ range from 23° to 127°, where 0° is consistent with a straight line through the center of a circular flux rope, indicating timing may provide the more precise estimate.

The tilts are consistent with previous statistical studies, showing axial directions are confined to the $\hat{x}_{GSM} - \hat{y}_{GSM}$ plane with a wide range of angles in this plane (Slavin, Lepping, Gjerloev, Fairfield, et al., 2003). Global simulations also show large tilts near the x-line (Lu, Lin, et al., 2015; Lu, Lu, et al., 2015). However, in contrast to the present study, previous observations of sequential tailward propagating flux ropes have found smaller tilts (<45°) with less variability within a given set of sequential flux ropes (Hietala et al., 2014; Kiehas et al., 2012).

The observations here, showing significant variability in orientation close to the x-line, indicate spatiotemporal variability in the reconnection or subsequent dynamics, such as rotation or kinking, of the flux ropes as they propagate away from the x-line.

Assuming cylindrical symmetry, the velocity perpendicular to the axial direction can be estimated using timing analysis on the peak |**B**|, which is done by correlating the signals from each spacecraft (Eastwood et al., 2016). Combined with the flux rope duration, taken to be the shaded intervals in Figures 2a–2d, these velocities give lower bounds on the flux rope sizes. Velocities and sizes are given in columns 6–8 of Table 1. The flux ropes are traveling broadly Earthward, although with significant $\hat{y}_{GSM}$ and $\hat{z}_{GSM}$ components, and sizes are consistent with ion scale flux ropes. The velocities slightly overestimate FPI $\mathbf{V}_i$ measurements of 170–350 km/s perpendicular to the axes, consistent with FPI underestimating $\mathbf{V}_i$ as mentioned above. Normal directions obtained from this analysis are roughly perpendicular to the axes found in the previous analyses (within 20° for MVA and 8° for timing), as expected.

4. Small-Scale Substructure

Spectrograms of high frequency (>10 Hz) **E** fluctuations (Figures 2b and 2g) reveal all three flux ropes show enhanced **E** power above that of the ambient plasma, as noted in other studies (Kennel et al., 1986; Øieroset et al., 2014; Wang et al., 2016). The **E** activity extends up to the electron plasma frequency, and localized enhancements in time and frequency are present. Similar enhancements in high-frequency magnetic fluctuations are not present, indicating largely electrostatic behavior. However, localized enhancements in magnetic fluctuations are present, for example, on the outgoing edge of FR1 between 100 and 200 Hz (Figure 2h) and ingoing boundary of FR3 at ~50 Hz, associated with localized electron heating in the perpendicular and parallel directions, respectively. We focus on the detailed analysis of one of the most intense **E**, which is associated with an electron vortex.

4.1. Electron-Scale Vortex

In Figures 2e and 2f, the intense **E**, observed between 22:35:08 and 22:35:09 UTC, is associated with a small-scale enhancement in axial **B** and consequently |**B**|. **E** is largely perpendicular to the axial direction and is, in fact, perpendicular to the local **B**. Figure 3a plots the |**B**| perturbation with the larger-scale flux rope signature removed by a 1-s running average. Figures 3b and 3c plot the components of **E** perpendicular to the local **B**. In this coordinate system, $\hat{\mathbb{1}}_1 \sim \hat{z}_{GSM}$ and $\hat{\mathbb{1}}_2 \sim \hat{x}_{GSM}$. The most intense **E**, in the $-\hat{\mathbb{1}}_1$ direction, is associated with the leading edge of the magnetic perturbation, while a less intense **E** in the $(\hat{\mathbb{1}}_1, -\hat{\mathbb{1}}_2)$ direction is associated with the trailing edge. A component of **J** parallel to **B** is expected within a flux rope and is present on large scales compared to the intense **E**. However, a perpendicular **J** is present, carried predominantly by electrons, with a similar profile to **E** but perpendicular to **E**, with the leading edge in the $-\hat{\mathbb{1}}_2$ direction and a weaker trailing edge in the $(+\hat{\mathbb{1}}_1, +\hat{\mathbb{1}}_2)$ direction as seen in Figures 3d and 3e.

Correlating $E_{\perp 1}$ from each spacecraft for the negative and positive peaks, corresponding to the leading and trailing edges of the structure, and performing timing analysis gives normal directions $\hat{\mathbf{n}}_- = [0.14, -0.07, -0.99]$ and $\hat{\mathbf{n}}_+ = [0.78, -0.02, -0.63]$ in GSM coordinates. The relative orientation of $\hat{\mathbf{n}}_-$ and $\hat{\mathbf{n}}_+$ along with the $\mathbf{J}_\perp$ orientations is consistent with a perpendicular current loop as illustrated in Figure 3h. Figures 3f and 3g plot **E** at the resolution of $\mathbf{V}_e$, $-\mathbf{V}_e \times \mathbf{B}$ and $-\mathbf{V}_i \times \mathbf{B}$, demonstrating **B** is decoupled from the ions and largely frozen-in to the electrons. Other terms from Ohm's law, such as the divergence of electron pressure (not shown), do not show significant signals above the noise. As **J** is carried by electrons, evident in Figures 1e–1j, this structure corresponds to an electron vortex. Based on timing velocities, current layer thicknesses are ~40 km ($2.5d_e$ or $4\rho_e$) on both the leading and trailing boundaries, and the full structure is ~160 km ($10d_e$ or $16\rho_e$). While the vortex has a magnetic enhancement, similar to a flux rope, the vortex itself does not contain a helical **B** and contains significant $\mathbf{J}_\perp$, making it a distinct type of structure.

The small size, which is much less than d_i and slightly larger than d_e, and fact $\mathbf{J}_\perp$ is perpendicular to **E** suggest $\mathbf{J}_\perp$ is carried by $\mathbf{E} \times \mathbf{B}$ drifting electrons. Since the scale of **E** is much less than the ion scales, the ions are decoupled from **E** allowing the $\mathbf{E} \times \mathbf{B}$ drift to drive a current. Such dynamics are fundamentally associated with the Hall term in Ohm's law. Assuming **J** is purely associated with an electron, $\mathbf{E} \times \mathbf{B}$ drift gives $\mathbf{J}_{E\times B} = -qn_e\mathbf{E} \times \mathbf{B}/|\mathbf{B}|^2$, where **E** is in the bulk plasma frame. Figures 3d and 3e plot $\mathbf{J}_{E\times B}$ in red. The transformation of **E** to the bulk plasma frame makes a negligible contribution in this case. In both $\mathbf{J}_\perp$ components, peaks associated with the electron vortex show good agreement between the measured **J** and $\mathbf{J}_{E\times B}$.

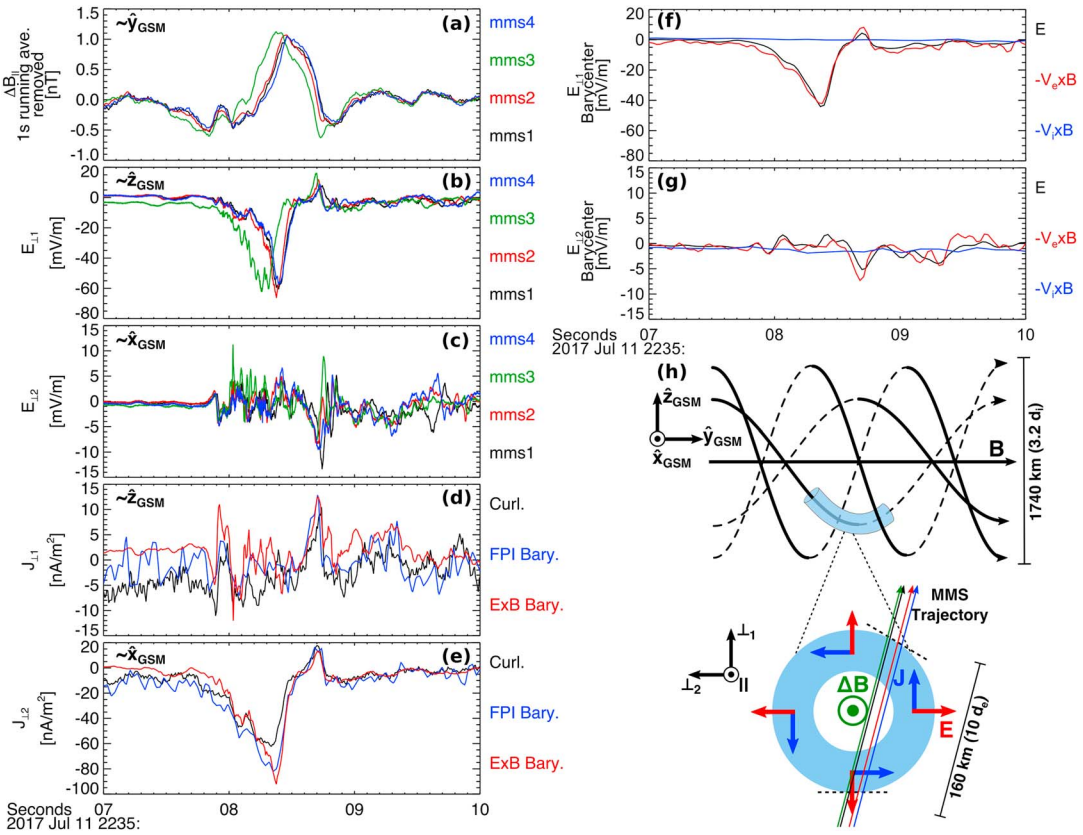

Figure 3. Enlarged view of the electron vortex, showing (a) the perturbation in **B** with a 1-s running average removed as observed by the four spacecraft, (b and c) perpendicular components of **E** as observed by the four spacecraft, and (d and e) perpendicular components of **J** computed from the curlometer (1/128-s cadence, black), Fast Plasma Investigation moments (0.03-s cadence, blue), and assuming **J** is due to an electron **E** × **B** drift (1/128-s cadence, red). The latter two **J** estimates are averaged to the barycenter. (f and g) Perpendicular components of **E**, $-V_i \times B$ and $-V_e \times B$ averaged to the barycenter. **E** and $-V_e \times B$ are filtered to 8 Hz to reduce noise. (h) Diagram of the electron-scale vortex encountered within flux rope 1. GSM = geocentric solar magnetospheric; MMS = Magnetospheric Multiscale; FPI = Fast Plasma Investigation.

The asymmetry in the vortex, noted above, is likely associated with the large-scale gradient in **B** due to the flux rope. As seen in Figure 2e, the total |**B**| perturbation is larger on the ingoing boundary, associated with the larger **E**, than on the outgoing boundary, associated with the smaller **E**. Since the current layer thickness is roughly the same on both boundaries, the asymmetry to the magnetic perturbation will cause such an asymmetry in **J** and **E**.

The MMS formation is over 10 times smaller than the vortex, evident in the nearly identical profiles for the spacecraft in Figures 3a–3c, which limits knowledge of the vortex shape. One observed difference between the spacecraft, particularly on the outgoing boundary, is the orientation of **E** in the $\hat{\perp}_1 - \hat{\perp}_2$ plane, ranging from 31° for MMS1 to 67° for MMS3 relative to $-\hat{\perp}_2$. Assuming **E** is normal to the boundary and given the relative spacecraft locations, the angles are consistent with a curved boundary as illustrated in Figure 3h, particularly for MMS2–4. MMS1 crossed the boundary last and is shallower than expected, which could relate to deformation from a circular shape, temporal variation, and/or the detailed trajectory through the structure. It is difficult to separate these possibilities given the small formation size relative to the vortex.

The electron vortex is reminiscent of small-scale magnetic holes, observed extensively in the plasma sheet (Gershman et al., 2016; Goodrich, Ergun, & Stawarz, 2016; Goodrich, Ergun, Wilder, et al., 2016), magnetosheath (Huang, Du, et al., 2017; Huang, Sahraoui, et al., 2017; Yao et al., 2017), and kinetic simulations (Haynes et al., 2015). In these structures, electron-scale current loops generate depletions in |**B**|, and similar to the structure observed here, **J** in some cases is linked to electron **E** × **B** drifts (Goodrich, Ergun, & Stawarz, 2016). However, a key difference here is that the vortex causes a magnetic enhancement instead of a depletion. It is possible the structure observed here is the analog of a magnetic hole with reversed polarity. Magnetic enhancements associated with small-scale current loops have not been as extensively discussed in the literature. However,

recent MMS observations near the magnetopause report electron scale magnetic enhancements (Yao et al., 2018), although the behavior of **E** is not examined.

Magnetic enhancements have also been studied theoretically (Tao et al., 2011; Treumann & Baumjohann, 2012) and observed (Andersson et al., 2009; Le Contel et al., 2017) in association with electron phase-space holes. In these structures, a net charge density caused by the phase-space hole drives a radial **E** and azimuthal **J** via an **E** × **B** drift (Treumann & Baumjohann, 2012). Electron phase-space holes, associated with positive charge density, generate an enhancement in **B**, while ion phase-space holes cause a depletion. However, phase-space holes often have a bipolar $E_{||}$ in observations due to fast propagation along **B** (e.g., Andersson et al., 2009; Ergun et al., 1998), which is not observed in this structure. A local depletion in n_e is associated with the electron vortex. However, based on the thickness of the vortex boundaries and Gauss's law with an assumed linear gradient, the necessary difference between ion and electron number density to produce the observed **E** is $\sim 10^{-4}$ cm^{-3}, and the particle measurements are not accurate enough to confirm such a charge separation.

The observed vortex does not exhibit a clear signature to infer the propagation velocity and length scale along **B**. The lack of $E_{||}$ and fact that timing analysis indicates boundaries perpendicular to **B** may indicate the structure is extended along **B**. However, the parallel length can only be constrained as larger than the ~15-km spacecraft separation.

B is frozen-in to the electron flow within the vortex such that **B** will be entrained by the vortical motion. At the structure's ends, where there is a boundary between vortical and nonvortical motion, nonfrozen-in behavior and an $E_{||}$ are necessary to decouple the structure from the surrounding plasma, which may impact particle acceleration. The strength of $E_{||}$ is unclear since the parallel gradients are not known; however, integrating $\mathbf{E}_{\perp}$ on the ingoing and outgoing boundaries using the timing velocities gives changes in electric potential of ~1,800 and 500 V, respectively.

Twisting of **B** at the structure's ends would occur on the timescale of the vortex making one rotation. Taking the diameter as 160 km with V_e observed to be ~5,000 km/s gives a vortex turnover time of ~0.1 s. Enhanced **E** and **B** power at ~10 Hz is associated with the electron vortex in Figures 2g and 2h, which may indicate waves driven by the vortex. Fluxgate magnetometer spectrograms (not shown) also confirm a peak at ~10 Hz.

5. Conclusions

We report novel observations of an electron-scale vortex within a flux rope in Earth's magnetotail. The vortex has an intense perpendicular **E**, directed radially outward from the vortex, and a vortical perpendicular current carried by **E** × **B** drifting electrons. The physics is similar to small-scale magnetic holes but with a magnetic enhancement instead of a depletion. While strong **E** have been previously reported within flux ropes, the unique capabilities of MMS enable a detailed examination of the electron-scale structure, which has not been previously possible.

Both the flux rope containing the electron vortex and the two nearby flux ropes are ion-scale structures, observed in close proximity (within 3 min) of an EDR reported by Torbert et al. (2017). The orientation of the flux rope axes is variable, with one flux rope oriented more along the cross-tail direction and the other two more toward the Earthward-tailward direction. This variability indicates potential spatiotemporal variability in the reconnection or subsequent dynamics and the necessity of three-dimensional simulations to model the system.

The results of this study prompt important questions about the substructure of flux ropes. How common are electron vortices within flux ropes and does their prevalence depend on plasma parameters? The vortex observed here was within a magnetotail flux rope; however, do they also occur within magnetopause flux ropes? Answering these questions will place constraints on the formation and stability of electron vortices. Additionally, simulations will help determine how such vortices are formed. A number of mechanisms may lead to the formation of magnetic holes (Sundberg et al., 2015), and the mechanisms that form electron vortices with magnetic enhancements are further unknown. Finally, the stability of these structures and their role in particle acceleration requires investigation. This study suggests these vortices may excite waves, and $E_{||}$ at the ends of these structures along **B** may accelerate particles. Such processes should be considered in understanding the energetics of flux ropes and reconnection outflows.

Acknowledgments
This work is supported by STFC (UK) grant ST/N000692/1. K. J. Genestreti is supported by the Austrian FFG project 847969, and D. Burgess is supported by STFC(UK) grant ST/P000622/1. The French involvement (SCM) on MMS is supported by CNES and CNRS. The authors gratefully acknowledge the ISSI International Team "Plasma Heating and Acceleration by Collisionless Magnetic Reconnection" where numerous discussions and collaborations developed and the MMS team for their work on the mission. Data are publicly available from the MMS Science Data Center (http://lasp.colorado.edu/mms/sdc/public/) and were analyzed using the SPEDAS software package for IDL (http://themis.ssl.berkeley.edu/software.shtml).

References

Andersson, L., Ergun, R. E., Tao, J., Roux, A., Lecontel, O., Angelopoulos, V., et al. (2009). New features of electron phase space holes observed by the THEMIS mission. *Physical Review Letters*, *102*(22), 225004. https://doi.org/10.1103/PhysRevLett.102.225004

Borg, A. L., Taylor, M. G. G. T., & Eastwood, J. P. (2012). Observations of magnetic flux ropes during magnetic reconnection in the Earth's magnetotail. *Annals of Geophysics*, *30*, 761–773. https://doi.org/10.5194/angeo-30-761-2012

Burch, J. L., Moore, T. E., Torbert, R. B., & Giles, B. L. (2016). Magnetospheric Multiscale overview and science objectives. *Space Science Reviews*, *199*, 5–21. https://doi.org/10.1007/s11214-015-0164-9

Chen, L.-J., Bhattacharjee, A., Puhl-Quinn, P. A., Yang, H., Bessho, N., Imada, S., et al. (2008). Observation of energetic electrons within magnetic islands. *Nature Physics*, *4*, 19–23. https://doi.org/10.1038/nphys777

Chen, L.-J., Daughton, W., Bhattacharjee, A., Torbert, R. B., Roytershteyn, V., & Bessho, N. (2012). In-plane electric fields in magnetic islands during collisionless magnetic reconnection. *Physics of Plasmas*, *19*(11), 112902. https://doi.org/10.1063/1.4767645

Dahlin, J. T., Drake, J. F., & Swisdak, M. (2017). The role of three-dimensional transport in driving enhanced electron acceleration during magnetic reconnection. *Physics of Plasmas*, *24*(9), 092110. https://doi.org/10.1063/1.4986211

Daughton, W., Scudder, J., & Karimabadi, H. (2006). Fully kinetic simulations of undriven magnetic reconnection with open boundary conditions. *Physics of Plasmas*, *13*(7), 072101. https://doi.org/10.1063/1.2218817

Drake, J. F., Swisdak, M., Che, H., & Shay, M. A. (2006). Electron acceleration from contracting magnetic islands during reconnection. *Nature*, *443*, 553–556. https://doi.org/10.1038/nature05116

Drake, J. F., Swisdak, M., Schoeffler, K. M., Rogers, B. N., & Kobayashi, S. (2006). Formation of secondary islands during magnetic reconnection. *Geophysical Research Letters*, *33*, L13105. https://doi.org/10.1029/2006GL025957

Eastwood, J. P., & Kiehas, S. A. (2015). Origin and evolution of plasmoids and flux ropes in the magnetotails of Earth and Mars. In A. Keiling, et al. (Eds.), *Magnetotails in the solar system, Washington DC American Geophysical Union Geophysical Monograph Series* (Vol. 207, pp. 269–287). https://doi.org/10.1002/9781118842324.ch16

Eastwood, J. P., Phan, T. D., Cassak, P. A., Gershman, D. J., Haggerty, C., Malakit, K., et al. (2016). Ion-scale secondary flux ropes generated by magnetopause reconnection as resolved by MMS. *Geophysical Research Letters*, *43*, 4716–4724. https://doi.org/10.1002/2016GL068747

Eastwood, J. P., Phan, T. D., Fear, R. C., Sibeck, D. G., Angelopoulos, V., Øieroset, M., & Shay, M. A. (2012). Survival of flux transfer event (FTE) flux ropes far along the tail magnetopause. *Journal of Geophysical Research*, *117*, A08222. https://doi.org/10.1029/2012JA017722

Eastwood, J. P., Phan, T.-D., Mozer, F. S., Shay, M. A., Fujimoto, M., Retinò, A., et al. (2007). Multi-point observations of the Hall electromagnetic field and secondary island formation during magnetic reconnection. *Journal of Geophysical Research*, *112*, A06235. https://doi.org/10.1029/2006JA012158

Eastwood, J. P., Sibeck, D. G., Slavin, J. A., Goldstein, M. L., Lavraud, B., Sitnov, M., et al. (2005). Observations of multiple X-line structure in the Earth's magnetotail current sheet: A Cluster case study. *Geophysical Research Letters*, *32*, L11105. https://doi.org/10.1029/2005GL022509

Ergun, R. E., Carlson, C. W., McFadden, J. P., Mozer, F. S., Delory, G. T., Peria, W., et al. (1998). FAST satellite observations of large-amplitude solitary structures. *Geophysical Research Letters*, *25*, 2041–2044. https://doi.org/10.1029/98GL00636

Ergun, R. E., Tucker, S., Westfall, J., Goodrich, K. A., Malaspina, D. M., Summers, D., et al. (2016). The axial double probe and fields signal processing for the MMS mission. *Space Science Reviews*, *199*, 167–188. https://doi.org/10.1007/s11214-014-0115-x

Fear, R. C., Milan, S. E., Fazakerley, A. N., Lucek, E. A., Cowley, S. W. H., & Dandouras, I. (2008). The azimuthal extent of three flux transfer events. *Annals of Geophysics*, *26*, 2353–2369. https://doi.org/10.5194/angeo-26-2353-2008

Fermo, R. L., Drake, J. F., & Swisdak, M. (2012). Secondary magnetic islands generated by the Kelvin-Helmholtz instability in a reconnecting current sheet. *Physical Review Letters*, *108*(25), 255005. https://doi.org/10.1103/PhysRevLett.108.255005

Gershman, D. J., Dorelli, J. C., Viñas, A. F., Avanov, L. A., Gliese, U., Barrie, A. C., et al. (2016). Electron dynamics in a subproton-gyroscale magnetic hole. *Geophysical Research Letters*, *43*, 4112–4118. https://doi.org/10.1002/2016GL068545

Goodrich, K. A., Ergun, R. E., & Stawarz, J. E. (2016). Electric fields associated with small-scale magnetic holes in the plasma sheet: Evidence for electron currents. *Geophysical Research Letters*, *43*, 6044–6050. https://doi.org/10.1002/2016GL069601

Goodrich, K. A., Ergun, R. E., Wilder, F. D., Burch, J., Torbert, R., Khotyaintsev, Y., et al. (2016). MMS multipoint electric field observations of small-scale magnetic holes. *Geophysical Research Letters*, *43*, 5953–5959. https://doi.org/10.1002/2016GL069157

Haynes, C. T., Burgess, D., Camporeale, E., & Sundberg, T. (2015). Electron vortex magnetic holes: A nonlinear coherent plasma structure. *Physics of Plasmas*, *22*(1), 012309. https://doi.org/10.1063/1.4906356

Hietala, H., Eastwood, J. P., & Isavnin, A. (2014). Sequentially released tilted flux ropes in the Earth's magnetotail. *Plasma Physics and Controlled Fusion*, *56*(6), 064011. https://doi.org/10.1088/0741-3335/56/6/064011

Hones Jr, E. W. (1977). Substorm processes in the magnetotail—Comments on 'On hot tenuous plasmas, fireballs, and boundary layers in the earth's magnetotail' by L. A. Frank, K. L. Ackerson, and R. P. Lepping. *Journal of Geophysical Research*, *82*, 5633–5640. https://doi.org/10.1029/JA082i035p05633

Huang, S. Y., Du, J. W., Sahraoui, F., Yuan, Z. G., He, J. S., Zhao, J. S., et al. (2017). A statistical study of kinetic-size magnetic holes in turbulent magnetosheath: MMS observations. *Journal of Geophysical Research: Space Physics*, *122*, 8577–8588. https://doi.org/10.1002/2017JA024415

Huang, S. Y., Sahraoui, F., Yuan, Z. G., He, J. S., Zhao, J. S., Le Contel, O., et al. (2017). Magnetospheric Multiscale observations of electron vortex magnetic hole in the turbulent magnetosheath plasma. *The Astrophysical Journal*, *836*(L27), 8. https://doi.org/10.3847/2041-8213/aa5f50

Huang, S. Y., Zhou, M., Yuan, Z. G., Deng, X. H., Sahraoui, F., Pang, Y., & Fu, S. (2014). Kinetic simulations of electric field structure within magnetic island during magnetic reconnection and their applications to the satellite observations. *Journal of Geophysical Research: Space Physics*, *119*, 7402–7412. https://doi.org/10.1002/2014JA020054

Hughes, W. J., & Sibeck, D. G. (1987). On the 3-dimensional structure of plasmoids. *Geophysical Research Letters*, *14*, 636–639. https://doi.org/10.1029/GL014i006p00636

Kennel, C. F., Coroniti, F. V., & Scarf, F. L. (1986). Plasma waves in magnetotail flux ropes. *Journal of Geophysical Research*, *91*, 1424–1438. https://doi.org/10.1029/JA091iA02p01424

Kiehas, S. A., Angelopoulos, V., Runov, A., Moldwin, M. B., & Möstl, C. (2012). On the formation of tilted flux ropes in the Earth's magnetotail observed with ARTEMIS. *Journal of Geophysical Research*, *117*, A05231. https://doi.org/10.1029/2011JA017377

Le Contel, O., Leroy, P., Roux, A., Coillot, C., Alison, D., Bouabdellah, A., et al. (2016). The search-coil magnetometer for MMS. *Space Science Reviews*, *199*, 257–282. https://doi.org/10.1007/s11214-014-0096-9.

Le Contel, O., Nakamura, R., Breuillard, H., Argall, M. R., Graham, D. B., Fischer, D., et al. (2017). Lower hybrid drift waves and electromagnetic electron space-phase holes associated with dipolarization fronts and field-aligned currents observed by the Magnetospheric Multiscale mission during a substorm. *Journal of Geophysical Research: Space Physics*, *122*, 12,236–12,257. https://doi.org/10.1002/2017JA024550

Lepping, R. P., Burlaga, L. F., & Jones, J. A. (1990). Magnetic field structure of interplanetary magnetic clouds at 1 AU. *Journal of Geophysical Research*, *95*, 11,957–11,965. https://doi.org/10.1029/JA095iA08p11957
Lindqvist, P.-A., Olsson, G., Torbert, R. B., King, B., Granoff, M., Rau, D., et al. (2016). The spin-plane double probe electric field instrument for MMS. *Space Science Reviews*, *199*, 137–165. https://doi.org/10.1007/s11214-014-0116-9
Lu, S., Lin, Y., Lu, Q. M., Wang, X. Y., Wang, R. S., Huang, C., et al. (2015). Evolution of flux ropes in the magnetotail: A three-dimensional global hybrid simulation. *Physics of Plasmas*, *22*(5), 052901. https://doi.org/10.1063/1.4919615
Lu, S., Lu, Q., Lin, Y., Wang, X., Ge, Y., Wang, R., et al. (2015). Dipolarization fronts as Earthward propagating flux ropes: A three-dimensional global hybrid simulation. *Journal of Geophysical Research: Space Physics*, *120*, 6286–6300. https://doi.org/10.1002/2015JA021213
Lundquist, S. (1950). Magnetohydrostatic fields. *Arkiv foer Physik*, *2*, 361.
Øieroset, M., Sundkvist, D., Chaston, C. C., Phan, T. D., Mozer, F. S., McFadden, J. P., et al. (2014). Observations of plasma waves in the colliding jet region of a magnetic flux rope flanked by two active X lines at the subsolar magnetopause. *Journal of Geophysical Research: Space Physics*, *119*, 6256–6272. https://doi.org/10.1002/2014JA020124
Pollock, C., Moore, T., Jacques, A., Burch, J., Gliese, U., Saito, Y., et al. (2016). Fast plasma investigation for Magnetospheric Multiscale. *Space Science Reviews*, *199*, 331–406. https://doi.org/10.1007/s11214-016-0245-4
Robert, P., Dunlop, M. W., Roux, A., & Chanteur, G. (1998). Accuracy of current density determination. *ISSI Scientific Reports Series*, *1*, 395–418.
Russell, C. T., Anderson, B. J., Baumjohann, W., Bromund, K. R., Dearborn, D., Fischer, D., et al. (2016). The Magnetospheric Multiscale magnetometers. *Space Science Reviews*, *199*, 189–256. https://doi.org/10.1007/s11214-014-0057-3
Schwartz, S. J. (1998). Shock and discontinuity normals, mach numbers, and related parameters. *ISSI Scientific Reports Series*, *1*, 249–270.
Sergeev, V. A., Angelopoulos, V., & Nakamura, R. (2012). Recent advances in understanding substorm dynamics. *Geophysical Research Letters*, *39*, L05101. https://doi.org/10.1029/2012GL050859
Sharma, A. S., Nakamura, R., Runov, A., Grigorenko, E. E., Hasegawa, H., Hoshino, M., et al. (2008). Transient and localized processes in the magnetotail: A review. *Annals of Geophysics*, *26*, 955–1006. https://doi.org/10.5194/angeo-26-955-2008
Shay, M. A., Drake, J. F., Eastwood, J. P., & Phan, T. D. (2011). Super-Alfvénic propagation of substorm reconnection signatures and Poynting flux. *Physical Review Letters*, *107*(6), 065001. https://doi.org/10.1103/PhysRevLett.107.065001
Slavin, J. A., Lepping, R. P., Gjerloev, J., Fairfield, D. H., Hesse, M., Owen, C. J., et al. (2003). Geotail observations of magnetic flux ropes in the plasma sheet. *Journal of Geophysical Research*, *108*, 1015. https://doi.org/10.1029/2002JA009557
Slavin, J. A., Lepping, R. P., Gjerloev, J., Goldstein, M. L., Fairfield, D. H., Acuna, M. H., et al. (2003). Cluster electric current density measurements within a magnetic flux rope in the plasma sheet. *Geophysical Research Letters*, *30*, 1362. https://doi.org/10.1029/2002GL016411
Sonnerup, B. U. Ö., & Scheible, M. (1998). Minimum and maximum variance analysis. *ISSI Scientific Reports Series*, *1*, 185–220.
Stawarz, J. E., Eastwood, J. P., Varsani, A., Ergun, R. E., Shay, M. A., Nakamura, R., et al. (2017). Magnetospheric Multiscale analysis of intense field-aligned Poynting flux near the Earth's plasma sheet boundary. *Geophysical Research Letters*, *44*, 7106–7113. https://doi.org/10.1002/2017GL073685
Stawarz, J. E., Ergun, R. E., & Goodrich, K. A. (2015). Generation of high-frequency electric field activity by turbulence in the Earth's magnetotail. *Journal of Geophysical Research: Space Physics*, *120*, 1845–1866. https://doi.org/10.1002/2014JA020166
Sundberg, T., Burgess, D., & Haynes, C. T. (2015). Properties and origin of subproton-scale magnetic holes in the terrestrial plasma sheet. *Journal of Geophysical Research: Space Physics*, *120*, 2600–2615. https://doi.org/10.1002/2014JA020856
Tao, J. B., Ergun, R. E., Andersson, L., Bonnell, J. W., Roux, A., Le Contel, O., et al. (2011). A model of electromagnetic electron phase-space holes and its application. *Journal of Geophysical Research*, *116*, A11213. https://doi.org/10.1029/2010JA016054
Torbert, R. B., Burch, J. L., Argall, M. R., Farrugia, C. J., Alm, L., Dors, I., et al. (2017). MMS encounters with reconnection diffusion regions in the Earth's magnetotail. In *AGU Fall Meeting Abstracts*.
Treumann, R. A., & Baumjohann, W. (2012). Magnetic field amplification in electron phase-space holes and related effects. *Annals of Geophysics*, *30*, 711–724. https://doi.org/10.5194/angeo-30-711-2012
Wang, R., Lu, Q., Du, A., & Wang, S. (2010). In situ observations of a aecondary magnetic island in an ion diffusion region and associated energetic electrons. *Physical Review Letters*, *104*(17), 175003. https://doi.org/10.1103/PhysRevLett.104.175003
Wang, R., Lu, Q., Nakamura, R., Huang, C., Li, X., Wu, M., et al. (2016). Electrostatic and electromagnetic fluctuations detected inside magnetic flux ropes during magnetic reconnection. *Journal of Geophysical Research: Space Physics*, *121*, 9473–9482. https://doi.org/10.1002/2016JA022906
Yang, Y. Y., Shen, C., Zhang, Y. C., Rong, Z. J., Li, X., Dunlop, M., et al. (2014). The force-free configuration of flux ropes in geomagnetotail: Cluster observations. *Journal of Geophysical Research: Space Physics*, *119*, 6327–6341. https://doi.org/10.1002/2013JA019642
Yao, S. T., Shi, Q. Q., Guo, R. L., Yao, Z. H., Tian, A. M., Degeling, A. W., et al. (2018). Magnetospheric Multiscale observations of electron scale magnetic peak. *Geophysical Research Letters*, *45*, 527–537. https://doi.org/10.1002/2017GL075711
Yao, S. T., Wang, X. G., Shi, Q. Q., Pitkänen, T., Hamrin, M., Yao, Z. H., et al. (2017). Observations of kinetic-size magnetic holes in the magnetosheath. *Journal of Geophysical Research: Space Physics*, *122*, 1990–2000. https://doi.org/10.1002/2016JA023858
Young, D. T., Burch, J. L., Gomez, R. G., De Los Santos, A., Miller, G. P., Wilson, P., et al. (2016). Hot Plasma Composition Analyzer for the Magnetospheric Multiscale mission. *Space Science Reviews*, *199*, 407–470. https://doi.org/10.1007/s11214-014-0119-6
Zhou, M., Deng, X. H., & Huang, S. Y. (2012). Electric field structure inside the secondary island in the reconnection diffusion region. *Physics of Plasmas*, *19*(4), 042902. https://doi.org/10.1063/1.3700194